JOURNAL OF GEOPHYSICAL RESEARCH, VOL. 113, D03204, doi:10.1029/2007JD008438, 2008

Comparison of CERES-MODIS stratus cloud properties with ground-based measurements at the DOE ARM Southern Great Plains site

Xiquan Dong,[1] Patrick Minnis,[2] Baike Xi,[1] Sunny Sun-Mack,[3] and Yan Chen[3]

Received 19 January 2007; revised 29 October 2007; accepted 14 November 2007; published 14 February 2008.

[1] Overcast stratus cloud properties derived for the Clouds and the Earth's Radiant Energy System (CERES) project using Terra and Aqua Moderate Resolution Imaging Spectroradiometer (MODIS) data are compared with observations taken at the Department of Energy (DOE) Atmospheric Radiation Measurement (ARM) Southern Great Plains site from March 2000 through December 2004. Retrievals from ARM surface-based data were averaged over a 1-h interval centered at the time of each satellite overpass, and the CERES-MODIS cloud properties were averaged within a 30 km × 30 km box centered on the ARM SGP site. Two data sets were analyzed: all of the data (ALL), which include multilayered, single-layered, and slightly broken stratus decks and a subset, single-layered unbroken decks (SL). The CERES-MODIS effective cloud heights were determined from effective cloud temperature using a lapse rate method with the surface temperature specified as the 24-h mean surface air temperature. For SL stratus, they are, on average, within the ARM radar-lidar estimated cloud boundaries and are 0.534 ± 0.542 km and 0.108 ± 0.480 km lower than the cloud physical tops and centers, respectively, and are comparable for day and night observations. The mean differences and standard deviations are slightly larger for ALL data, but not statistically different to those of SL data. The MODIS-derived effective cloud temperatures are 2.7 ± 2.4 K less than the surface-observed SL cloud center temperatures with very high correlations (0.86–0.97). Variations in the height differences are mainly caused by uncertainties in the surface air temperatures, lapse rates, and cloud top height variability. The biases are mainly the result of the differences between effective and physical cloud top, which are governed by cloud liquid water content and viewing zenith angle, and the selected lapse rate, -7.1 K km^{-1}. On the basis of a total of 43 samples, the means and standard deviations of the differences between the daytime Terra and surface retrievals of effective radius r_e, optical depth, and liquid water path for SL stratus are 0.1 ± 1.9 μm (1.2 ± 23.5%), -1.3 ± 9.5 (-3.6 ± 26.2%), and 0.6 ± 49.9 gm^{-2} (0.3 ± 27%), respectively, while the corresponding correlation coefficients are 0.44, 0.87, and 0.89. For Aqua, they are 0.2 ± 1.9 μm (2.5 ± 23.4%), 2.5 ± 7.8 (7.8 ± 24.3%), and 28.1 ± 52.7 gm^{-2} (17.2 ± 32.2%), as well as 0.35, 0.96, and 0.93 from a total of 21 cases. The results for ALL cases are comparable. Although a bias in r_e was expected because the satellite retrieval of effective radius only represents the top of the cloud, the surface-based radar retrievals revealed that the vertical profile of r_e is highly variable with smaller droplets occurring at cloud top in some cases. The larger bias in optical depth and liquid water path for Aqua is due, at least partially, to differences in the Terra and Aqua MODIS visible channel calibrations. Methods for improving the cloud top height and microphysical property retrievals are suggested.

Citation: Dong, X., P. Minnis, B. Xi, S. Sun-Mack, and Y. Chen (2008), Comparison of CERES-MODIS stratus cloud properties with ground-based measurements at the DOE ARM Southern Great Plains site, *J. Geophys. Res.*, *113*, D03204, doi:10.1029/2007JD008438.

1. Introduction

[2] Clouds constitute one of the largest sources of uncertainty in predicting any potential future climate change [*Wielicki et al.*, 1995; *Houghton et al.*, 2001]. Thus assessment of their interactions with the Earth's radiation budget and accurate representation of clouds in climate models have been classified as the highest priority by the U.S.

[1] Department of Atmospheric Sciences, University of North Dakota, Grand Forks, North Dakota, USA.
[2] NASA Langley Research Center, Hampton, Virginia, USA.
[3] Science Applications International Corporation, Inc., Hampton, Virginia, USA.

0148-0227/08/2007JD008438$09.00

Climate Change Research Initiative (USCCRI 2001, see http://www.climatescience.gov/about/ccri.htm). The impact of clouds on the radiation budget mainly depends on cloud amount and height, cloud particle size and shape, and cloud (or ice) water content [e.g., *Curry et al.*, 2000; *Houghton et al.*, 2001]. This impact is highlighted by the wide range of cloud feedback results found in the *Cess et al.* [1990] intercomparison of 19 general circulation models (GCMs) that represented cloud microphysical and radiative processes in a variety of ways. The range of results narrowed as the cloud properties used in the models were altered [*Cess et al.*, 1996a]. Ultimately, the models should reproduce the cloud properties that are observed. Thus global satellite data are critical for both verifying and improving GCM cloud parameterizations for climate prediction. Proper application of those data to climate questions requires a reasonable characterization of their uncertainties.

[3] The NASA Clouds and the Earth's Radiant Energy System (CERES) project provides the first long-term global simultaneous measurements necessary for estimating the Earth's broadband radiation budget and retrieving cloud properties to achieve consistent radiative fluxes from the surface to the top of the atmosphere (TOA) [*Wielicki et al.*, 1998]. The CERES project was designed with specific climate accuracy goals for TOA, surface, and atmosphere fluxes matched with surface, cloud, and aerosol data [*Wielicki et al.*, 1995, 1996]. The CERES cloud and radiative flux data products should dramatically improve our understanding of cloud-radiation interactions, particularly, cloud feedback effects on the Earth radiation balance. Therefore the CERES data should be useful for studying climate system forcings and feedbacks to answer critical scientific questions and to understand and improve climate change simulations because they can be used to constrain GCMs. However, the limits placed on the GCM output can be no tighter than the accuracy of the observations.

[4] Estimation of the errors in the derived cloud and radiative properties requires both theoretical evaluations of the measurement system capabilities and comparison with independent measurements of the same quantities. Ground-based measurements can provide independent "ground truth" data for estimating uncertainties in satellite-derived cloud properties, but they must first be properly analyzed and validated and their uncertainties must be understood. Comparisons between the ground- and satellite-based observations must be conducted carefully because of significant spatial and temporal differences between the two different observing platforms. Also because clouds are so variable, a statistically reliable validation requires coincident satellite-surface measurements taken in a variety of conditions. Complete validation of CERES cloud retrievals with independent ground truth observations should account for the following variables: (1) cloud types (low, middle, high, multiple layer, and broken), (2) surface types (ocean, vegetated land, nonvegetated land, mountains, snow covered land, and ice-covered water), (3) seasons, (4) day and night, and (5) viewing and illumination angles (e.g., satellite view zenith angle VZA, relative azimuth angle, and solar zenith angle SZA). A complete quantitative assessment requires at least 100 independent samples for each of the conditions, and the independent samples must be typically 100–300 km apart and separated by 6 to 12 h in time for clouds and radiation [*Wielicki et al.*, 2000]. Although the use of ground-based sensors, such as radar, lidar, and microwave radiometer, for validating satellite-derived cloud properties is well established [e.g., *Minnis et al.*, 1992, 1993b; *Mace et al.*, 1998, 2005; *Greenwald et al.*, 1999; *Dong et al.*, 2001, 2002], reference or ground truth data are currently limited both geographically and temporally to a few types of clouds over particular areas, or limited to case studies. These case studies cannot provide a statistically reliable validation for different types of clouds in various climatic regimes. Therefore complete validation of cloud retrievals in all conditions will take many years to achieve and will proceed in steps for particular conditions using the available reference data sets.

[5] This paper presents a comparison of stratus cloud properties derived from Moderate Resolution Imaging Spectroradiometer (MODIS) data for CERES with ground-based observations from March 2000 to December 2004 at the Department of Energy (DOE) Atmospheric Radiation Measurement (ARM) Program [*Ackerman and Stokes*, 2003] Southern Great Plains (SGP) site (36.6°N, 262.5°E). CERES single-layer cirrus cloud properties have been compared to radar and lidar-based observations in earlier studies [*Mace et al.*, 2005; *Chiriaco et al.*, 2007]. Here, low-level stratus cloud macrophysical and microphysical properties derived from the MODIS on Terra and Aqua as part of the CERES project are compared to simultaneous ground-based observations. Note, that these cloud properties are not those derived by the MODIS Atmospheres Science Team (MOD06 [*Platnick et al.*, 2003]), but are derived from MODIS data using entirely different algorithms [*Minnis et al.*, 2006]. Thus all MODIS results discussed here are those derived by the CERES Science Team. The surface data are used as a ground truth data set to validate the MODIS cloud properties and improve the CERES daytime and nighttime cloud retrieval algorithms. No attempt is made to exhaustively validate the CERES cloud retrieval algorithms; rather, our emphasis is to validate the CERES-derived properties of both daytime and nighttime single-layer and overcast stratus clouds over the ARM SGP site. We focus this study on single-layer and overcast stratus clouds because the clouds are the closest to plane-parallel and are well behaved. Thus the errors or biases in this study are most likely controlled by the spatial-temporal disparities from different sensors and different field of views. Comparisons of stratus at other locations and of other types of clouds, such as cirrus, overlapped, and broken clouds, will be undertaken as the surface retrieval algorithms are developed and verified by aircraft in situ measurements.

2. Data and Methods

[6] Since there are significant spatial and temporal differences between surface and satellite observations, such as the relatively small sizes of the surface radar/lidar field of view as compared to the much larger satellite field of view, temporal and spatial scales should be matched as closely as possible during the surface-satellite comparison. The surface data were averaged over a 1-h interval centered at the time of the satellite overpass, and the satellite data were averaged within a 30 km × 30 km area centered on the ARM SGP site. Note that for low-level winds of 10 m s^{-1},

Table 1. Surface- and Satellite-Derived Cloud Properties and Their Uncertainties

Cloud Property	Uncertainty	Instrument and Retrieval Algorithm
ARM H_{base}	~8 m	laser ceilometer or lidar or radar [*Clothiaux et al.*, 2000]
ARM H_{top}	90 m	microwave cloud radar (MMCR) [*Clothiaux et al.*, 2000; *Moran et al.*, 1998]
ARM T_{base} and T_{top}	0.2°C	Vaisala radiosonde
ARM r_e	~10% for daytime	*Dong et al.* [1997, 1998, 2002]
ARM τ	~5–10% for daytime	*Dong et al.* [1997, 1998, 2002]
ARM LWP	20 gm^{-2} $\langle$ LWP < 200 gm^{-2}, 20 gm^{-2}; LWP $\rangle$ 200 gm^{-2}, ~10%	LWP retrieved from microwave radiometer measured brightness temp [*Dong et al.*, 2000; *Liljegren et al.*, 2001]
MODIS T_e	<0.5 K for dry atmosphere, <1.0 K for moist atmosphere	*Minnis et al.* [1995]
MODIS H_e	<0.14 km for perfect sounding	*Minnis et al.* [2003]
MODIS r_e	15%	*Han et al.* [1994], *Platnick and Valero* [1995], *Minnis et al.* [1998]
MODIS τ	8%	*Platnick and Valero* [1995], *Minnis et al.* [1998]
MODIS LWP	17%	$(\Delta r_e^2 + \Delta\tau^2)^{1/2}$

the 1 h averaging interval used in this study is equivalent to a frozen turbulence spatial scale of 36 km. In a statistical context, the temporally averaged surface observations should be equivalent to the spatially averaged satellite results, as demonstrated by *Cess et al.* [1996b].

2.1. Surface

[7] The ARM ground-based observations and retrievals, as well as their uncertainties and references used in this study, are listed in Table 1. The centerpiece of the cloud instrument array is the millimeter wavelength cloud radar (MMCR [*Moran et al.*, 1998]). The MMCR operates at a wavelength of 8 mm in a vertically pointing mode and provides continuous profiles of radar reflectivity from hydrometeors moving through the radar field of view, allowing the identification of clear and cloudy conditions. Cloud top height (H_{top}) is derived from cloud radar reflectivity profiles with an uncertainty of 90 m. To ensure that the MMCR estimate of cloud top height is not affected by flying insects, we compared cloud boundaries for several low-level cases during the spring, summer, and fall of 2006 using both MMCR and the new ARM 94-GHz radar (WACR) reflectivities at the SGP site. We found that the MMCR is indeed more sensitive to the presence of insects than the WACR below and/or in the clouds, but not near cloud top. Therefore we conclude that the MMCR-estimated cloud top heights are unaffected by flying insects. Cloud base height (H_{base}) is derived from a composite of Belfort laser ceilometer, micropulse lidar, and cloud radar data [*Clothiaux et al.*, 2000]. *Clothiaux et al.* [2000] summarized the current ARM methods to derive cloud boundaries using ARM radar-lidar data, as well as their uncertainties. Their methods produce the ARM MMCR and the active remote sensing of clouds (ARSCL) Value Added Products. The radar-lidar derived cloud boundaries have been partially validated by aircraft in situ measurements [*Dong et al.*, 1998, 2002; *Dong and Mace*, 2003].

[8] For comparison with the satellite data, which are referenced to mean sea level, 0.317 km was added to each surface-determined cloud height. Cloud base and cloud-top temperatures, T_{base} and T_{top}, are estimated from a linear temporal interpolation of ARM SCF rawinsonde soundings (~4 times per day) using H_{base} and H_{top}. The instantaneous soundings are first degraded to a common vertical resolution of 90 m before linear interpolation. The interpolated soundings, combined with other measurements and corrections, are denoted as ARM merged soundings. The cloud liquid water path (LWP) is derived from the microwave radiometer brightness temperatures measured at 23.8 and 31.4 GHz using a statistical retrieval method [*Liljegren et al.*, 2001].

[9] To retrieve daytime microphysical properties of single-layer and overcast stratus clouds in the midlatitudes, *Dong et al.* [1997] used a δ2-stream radiative transfer model in conjunction with ground-based measurements. The retrieval scheme is based on an iterative approach that varies cloud-droplet effective radius (r_e) in the radiative transfer calculations until the model-calculated solar transmission matches the measured value. *Dong et al.* [1998] parameterized the retrieved r_e as a function of LWP, the solar transmission, and cos(SZA), μ_0. The optical depth τ is derived from the ratio of LWP and r_e ($\tau \approx 1.5$*LWP/r_e). The retrieved and parameterized stratus cloud microphysical properties have been validated by in situ aircraft measurements in the midlatitudes [*Dong et al.*, 1998, 2002; *Dong and Mace*, 2003]. The uncertainties of the surface retrieved r_e, τ and LWP, listed in the Table 1, were estimated from approximately 5 h aircraft in situ measurements over the Pennsylvania State University surface site during 24 October 1998, and 10 h aircraft in situ measurements over the ARM SGP site during March 2000.

[10] Five criteria were established for choosing the conditions under which daytime surface cloud microphysical properties can be retrieved from the surface data. These criteria are (1) only single-layer and overcast low clouds are present as determined from cloud radar observations, (2) cloud top altitude H_{top} is less than 4 km, (3) the liquid water path LWP is between 20 and 700 g m^{-2}, (4) the cosine of solar zenith angle (μ_0) is larger than 0.2, and (5) the range of effective solar transmission (γ) is between 0.1 and 0.7. The physical reasons for using these five criteria were discussed by *Dong et al.* [2000]. Since some surface cloud cases have only height and temperature retrievals without microphysical retrievals because the clouds do not meet the retrieval criteria, the number of cases used in the cloud microphysical property comparison

is slightly less than that for the cloud height and temperature comparisons.

2.2. Satellite

[11] The satellite data sets used in this study are the Terra Edition2B and Aqua Edition1B 1-km pixel-level cloud properties that serve as input into the CERES Single Scanner Footprint (SSF) product. The SSF combines the CERES broadband flux measurements at a 20-km resolution with coincident, subsampled 1-km MODIS cloud and aerosol retrievals. The CERES cloud processing subsystem only analyzes every other pixel and every fourth scan line of the 1-km MODIS Collection-4 data. A set of algorithms and parameterizations [*Minnis et al.*, 1995, 1998, 2006] was developed to derive cloud phase, effective cloud height (H_{eff}) and temperature (T_{eff}), r_e or ice crystal effective diameter (D_e), τ, and LWP or ice water path (IWP) for each imager pixel that is classified as cloudy by the CERES cloud mask. Six cloud masks were developed to classify MODIS pixels for CERES as either cloudy or clear in nonpolar [*Trepte et al.*, 1999] and polar regions [*Trepte et al.*, 2002] during daytime (SZA $< 82°$), twilight ($82° \leq$ SZA $\leq 88.5°$), and nighttime (SZA $> 88.5°$). Each clear or cloudy pixel is further classified as "weak" or "strong" to indicate the degree of confidence in each pixel's classification. These masks use the 0.64 (VIS), 1.62, 3.78, 10.8 (IR), and 12.0-μm channels from MODIS.

2.2.1. Cloud Effective Height

[12] The effective temperature is defined as the brightness temperature corresponding to the 10.8-μm radiance,

$$L = (1 - \varepsilon)L_s + \varepsilon L_{eff}, \quad (1)$$

where L is the observed 10.8-μm radiance after correction for attenuation and emission of the overlaying atmosphere, L_s is the upwelling radiance at cloud base, and ε is the cloud effective emissivity and is a function of several variables, most notably, τ [*Minnis et al.*, 1998]. As τ approaches 4 or 5, the emissivity approaches unity and the radiance from the surface has no impact on the derived temperature.

[13] The primary technique for determining H_{eff} is to first estimate T_{eff} based on the IR radiance adjusted according to τ, and then determine H_{eff} using either of two methods. For low clouds, a simple lapse rate technique anchored to a surface temperature T_o is used [*Minnis and Harrison*, 1984; *Minnis et al.*, 1992]. That is,

$$H_{eff} = (T_{eff} - T_o)/\Gamma + H_o \quad (2)$$

where H_o is the surface elevation above mean sea level and Γ is the lapse rate. At the SGP, $H_o = 0.317$ km. Over ocean and land surfaces, the value of T_o is, respectively, the sea surface temperature and the running 24-h mean surface air temperature from the reanalyses provided by the Global Modeling Assimilation Office GEOS 4.03 [*Bloom et al.*, 2005]. Following *Minnis et al.* [2003], a lapse rate of -7.1 K km^{-1} is used between the surface and 700 hPa. Between 700 and 500 hPa, Γ is adjusted to ensure that the resulting temperature at 500 hPa equals that in the GEOS profile. For pressures less than 500 hPa, H_{eff} is defined as the lowest altitude having T_{eff} in the GEOS vertical profile of atmospheric temperature. If the initial atmospheric temperature (i.e., T_o) is less than T_{eff}, then the height is set, as a default, to 0.5 km. This condition occurred once in the data set used here.

[14] Most satellite retrieval algorithms convert T_{eff} to H_{eff} directly from a vertical temperature profile based on a sounding or a numerical weather prediction (NWP) model analysis [e.g., *Rossow and Schiffer*, 1999]. However, when a cloud forms underneath an inversion, the measured vertical profile often misses the coldest temperature under the inversion, likely as a result of the sharpness of the inversion and the relatively slow thermal response of the instrument [e.g., *Mahesh et al.*, 1997]. Additionally, in the case of NWP profiles, the minimum temperature under the inversion can be overestimated because of low vertical resolution, sparse input data, or parameterization errors. Thus, if either type of profile is used to convert T_{eff} to H_{eff}, the value of H_{eff} will frequently be greater than the true cloud top height [e.g., *Garreaud et al.*, 2001], as will be shown in this study. *Minnis et al.* [1992] developed the lapse rate approach to overcome the need for a vertical temperature profile that perfectly defines the temperature at the base of the marine boundary layer inversion. The CERES Terra Edition-1 processing [*Minnis et al.*, 2002] used the lapse rate method over ocean, but the sounding method over land employing temperature profiles from the European Center for Medium-Range Weather Forecasting (ECMWF) analyses. Comparisons of the retrieved stratus cloud heights with the MMCR data at the SGP revealed biases of 0.62 km in stratus cloud height. Thus the lapse rate used over ocean was tested and found to eliminate the bias over the SGP. Therefore the lapse rate approach, employing a value of -7.1 K km^{-1}, was used over both land and ocean in the CERES Terra Edition 2 and Aqua Edition 1 processing.

2.2.2. Microphysical Properties

[15] The main CERES daytime cloud microphysical retrieval algorithm is the 4-channel VISST (Visible Infrared Solar-Infrared Split-window Technique), an updated version of the 3-channel visible infrared solar-infrared method described by *Minnis et al.* [1995]. Given the spectral clear-sky radiances and surface properties for a particular set of SZA, VZA, and relative azimuth angles, the VISST computes the spectral radiances expected at TOA for both water droplet and ice crystal clouds over a range of optical depth from 0.25 to 128 for a particular cloud temperature. The values of r_e for the model clouds range from 2 to 32 μm [*Minnis et al.*, 1998]. The modeled TOA radiances include the attenuation of the radiation by the atmosphere and the impact of the radiation emitted or reflected by the surface. Atmospheric absorption is computed using the correlated *k*-distribution method of *Kratz* [1995] adapted to the MODIS channels [e.g., *Minnis et al.*, 2002] with the GEOS 4.03 profiles of temperature, humidity, ozone, and constant values for trace gases serving as input. Visible reflectance is estimated using the parameterization reported by *Arduini et al.* [2002], which accounts for Rayleigh scattering as in *Minnis et al.* [1993a]. VISST relies on the IR radiance to determine T_{eff}, the VIS reflectance to obtain τ, and the 3.7-μm radiance to estimate r_e. The split-window channel (12.0 μm) is used to help determine phase. These parameters are determined iteratively for each pixel by matching the observed radiances to TOA radiances calculated using emittance and reflectance parameterizations that account

for atmospheric attenuation and surface reflectance and emission [*Minnis et al.*, 1995, 1998]. Cloud LWP is then deduced from the combination of the retrieved τ and r_e as in the work by *Minnis et al.* [1998]. Given no information about the vertical profile of droplet radius, it is assumed that the derived value of r_e, which corresponds to the topmost portion of the cloud, represents the entire cloud as in the work by *Han et al.* [1994].

2.2.3. Uncertainties in Satellite Retrievals

[16] The uncertainties of the MODIS-retrieved cloud microphysical properties are also listed in Table 1. For clouds with $\tau > 4$, the uncertainty in T_{eff} is primarily dependent on the satellite calibration and the atmospheric corrections. In absolute terms, we expect the MODIS 10.8-μm calibration to be accurate to 0.03 ± 0.12 K [*Tobin et al.*, 2006]. The errors in the vertical profiles of humidity are difficult to fully assess. It is estimated that the uncertainty in the atmospheric emissivity is on the order of 25% resulting in a range of potential errors depending on the humidity of the atmosphere above the cloud. A maximum error of 1 K would result for a very moist atmosphere. At the SGP site, uncertainties less than 0.5 K are expected because the atmosphere above stratus clouds is often quite dry. If the assumed boundary layer lapse rate is correct, the error in cloud height from the uncertainty in T_{eff} would be less than 0.15 km. The height is also very sensitive to the boundary layer lapse rate ($\Delta H_{eff}/H_{eff} \sim -\Delta\Gamma/\Gamma$). For example, the derived H_{eff} values would be 41% higher using $\Gamma = -4$ K/km and 41% lower using $\Gamma = -10$ K/km than the H_{eff} using $\Gamma = -7.1$ K/km. Since cloud height is a second-order product, a theoretical error assessment is not particularly straightforward because of the complicated and variable structure of the lower atmosphere. One of the purposes of this study is to determine that error by comparison with a ground truth reference.

[17] The uncertainties in the cloud optical properties derived using the channels employed by the VISST have been explored in detail by *Han et al.* [1994] and *Platnick and Valero* [1995]. The estimates given here are deduced from their summaries and from analysis of the VISST input data and models. The retrieved optical depth is sensitive to errors in the input and algorithms; it varies with the magnitude of the optical depth. The parameterization used to determine optical depth from the VIS reflectance has an RMS error of ±0.5% relative to complete adding-doubling calculations [*Arduini et al.*, 2002] that translates to an optical depth uncertainty of ~1.7%. Uncertainties in the MODIS VIS channel reflectance and the background reflectance are expected to be on the order of ±2% and ±15%, respectively. For $\tau = 20$, the former translates to an optical depth error of ~7%, while the latter is roughly 2%. Uncertainties in the gaseous absorption in the VIS channel correspond to τ errors of about 3%. Assuming that these are random errors independent of each other, the overall uncertainty is roughly +8%. This value increases with increasing τ and decreases for smaller optical depths. The cloud droplet size is primarily based on the 3.7-μm reflectance, which is related to the brightness temperature difference (BTD) between the 3.7- and 10.8-μm channels. For optically thick clouds, the surface reflectance and emission have little impact on the BTD. The assumed size distribution variance causes an uncertainty of ~10% and in-cloud absorption adds another 3% [*Platnick and Valero*, 1995], while the potential range of solar constant for the MODIS 3.7-μm spectral band causes an uncertainty of ~5%. Because the atmospheric absorption errors track those of the 10.8-μm channel, the uncertainty in the 3.7-μm reflectance should be less than expected from a calculation considering only the 3.7-μm channel because the BTD changes much less with absorption errors than the absolute value of 3.7-μm radiance. The resulting reflectance error is expected to be ~10% leading to an overall uncertainty in r_e of 15%. Assuming that the uncertainties in τ and r_e are independent, then the uncertainty in the LWP should be ~17%.

3. Results

[18] An initial selection process based on the ARM radar-lidar observations and satellite data identified a total of 64 Terra daytime and 36 nighttime low-level and overcast stratus cases between March 2000 and December 2004. For Aqua, 45 daytime and 33 nighttime cases were identified in the same manner for data taken from July 2002 to December 2004 at the ARM SGP site. Additional examination of the satellite and radar imagery was then used to further screen the data to remove scenes with multiple layers of stratus clouds, any remaining overlying cirrus, slightly broken cloud fields, clouds with low optical depths, or snow covered surfaces. This process reduced the number of respective daytime and nighttime cases to 43 and 23 and to 22 and 24 for Terra and Aqua, respectively. Both data sets are considered here. The reduced data set, denoted hereafter as the single-layer (SL) data set comprises the purest single-layer and overcast cases and is examined separately because it minimizes the factors that can cause disagreement between the satellite and surface retrievals. It is a subset of the initial data sets and was selected using the following criteria: (1) optically thick clouds (both surface and MODIS averaged $\tau \geq 10$ and $\tau \geq 5$ for daytime and nighttime, respectively), (2) a continuous solid cloud layer observed from ARM radar-lidar observations within ±1 h of the satellite overpass, and (3) no cirrus or clear pixels within the 30 km × 30 km box from satellite images. The original data set, hereafter denoted as ALL, is also analyzed because it represents a wider range of overcast or nearly overcast stratus conditions observed by the satellite.

3.1. Cloud Height and Temperature Comparisons

[19] Figure 1 shows time series of H_{eff} and T_{eff} derived from Terra and Aqua SL data along with the surface-derived H_{base}/H_{top} and T_{base}/T_{top} for daytime stratus clouds at the ARM SGP site. The samples numbered in order from March 2000 through December 2004 and from July 2000 through December 2004 for Terra and Aqua, respectively. In most instances, the mean and standard deviations ($\pm 1\sigma$) of Terra H_{eff} fall between H_{top} and H_{base} (Figure 1a). The corresponding values of T_{eff} tend to be 2–5 K less than their T_{top} and T_{base} counterparts for those same samples (Figure 1c). Scatterplots of H_{eff} versus H_{top} and H_{mean} and of T_{eff} versus T_{top} and T_{mean} are given in Figures 2a and 2b. The parameters, H_{mean} and T_{mean}, correspond to the altitude and temperature at the center of the cloud, respectively. Despite the relatively close tracking of the satellite and surface-derived heights in Figure 1a, the correlation coef-

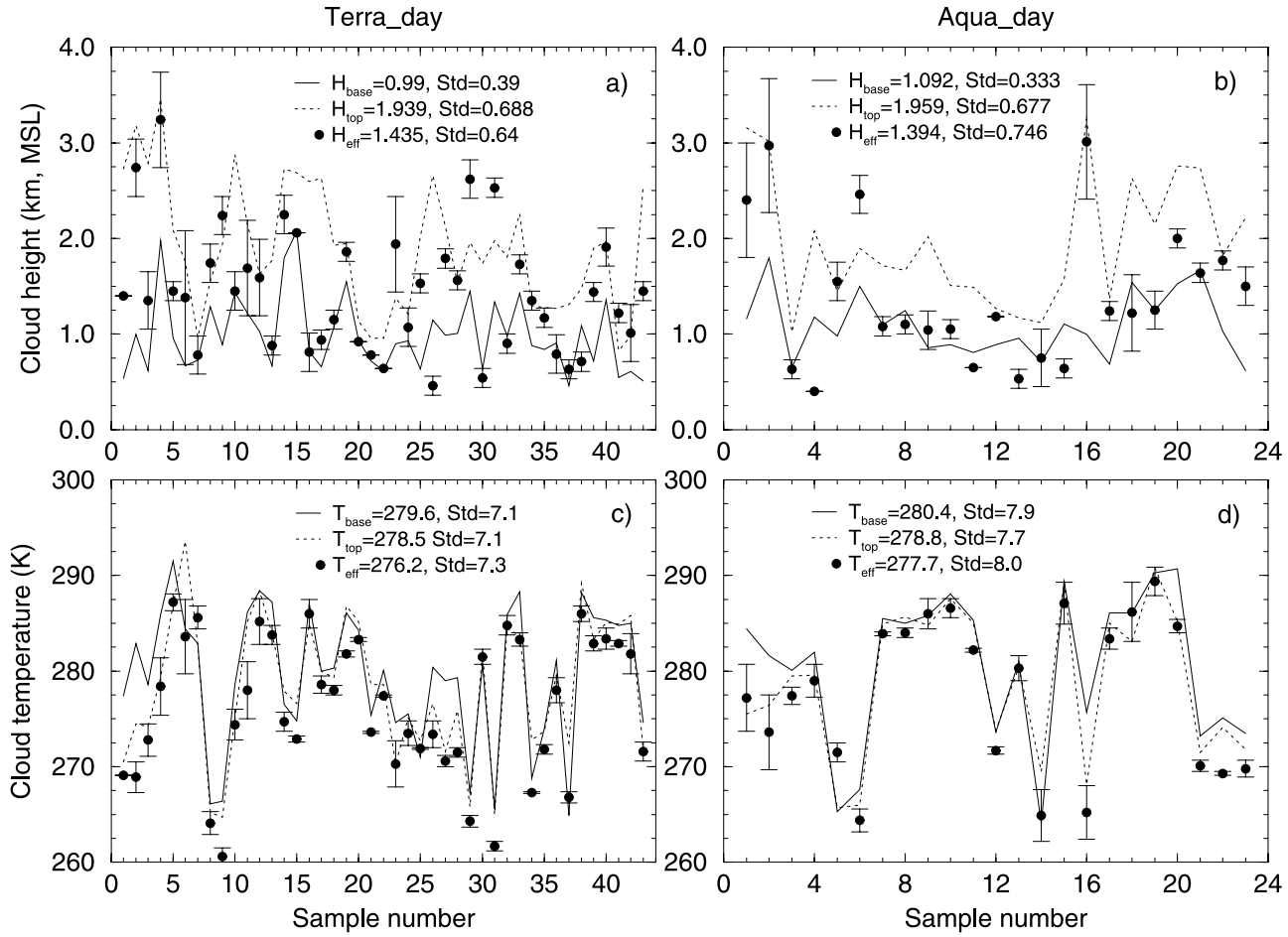

Figure 1. Time series of surface-derived cloud base and cloud-top (a and b) heights and (c and d) temperatures (1-h average) and matched MODIS-derived effective cloud heights and temperatures (30 km × 30 km box) for daytime single-layer and overcast stratus clouds over the ARM SGP site (sample number is ordered from March 2000 to December 2004 for Terra and from July 2002 to December 2004 for Aqua). Error bars denote standard deviations ($\pm 1\sigma$) of MODIS parameters.

ficients only range between 0.535 and 0.585 (Figure 2a). The satellite and surface-derived cloud temperatures (Figure 2b) are much better correlated, ~0.95, than their height counterparts.

[20] Time series of H_{eff} and T_{eff} from Aqua during July 2002 through December 2004 are shown in Figures 1b and 1d with the corresponding surface-derived values of H_{base}/H_{top} and T_{base}/T_{top} for daytime cases at the ARM SGP site. The scatterplots for those same data are shown in Figures 2c and 2d. The averaged Aqua T_{eff} and H_{eff} values are 1.1 K and 0.565 km less than T_{top} and H_{top} (Figures 2c and 2d), respectively, while the mean H_{eff} is 0.131 km less than and 0.302 km greater than the average values of H_{mean} and H_{base}, respectively (Table 2). Compared to the Terra results, fewer H_{eff} values are within the radar-lidar derived cloud boundaries and scatter around the cloud center (Figure 1b); more of them fall below cloud base. The correlation coefficients between the satellite and surface-determined temperatures (~0.95) in Table 2 are greater than those between H_{eff} and H_{top}/H_{mean} (~0.74). The standard deviations (SD) of the height and temperature differences in Table 2 are comparable to their Terra counterparts.

[21] Time series and scatterplots of the SL nighttime cloud heights and temperatures are shown in Figures 3 and 4, respectively. As demonstrated in Figures 3 and 4 and in Table 2, the nighttime satellite retrievals are similar to their daytime counterparts relative to the ARM observations with slightly more cases near cloud base. On average, H_{eff} is about halfway between the middle and base of the clouds. As in the daytime cases, the averaged Terra and Aqua T_{eff} values are typically a few degrees lower than the mean T_{top} values and their correlations with T_{top} and T_{mean} are 0.97 and 0.88, respectively. The correlations between H_{eff} and H_{top}/H_{mean} during nighttime (~0.71) seen in Figures 4a and 4c are slightly greater than those during daytime (~0.65). Table 2 summarizes the comparisons. These results should be a good representation of the biases between the satellite and surface retrievals of stratus cloud heights and temperatures at the ARM SGP site.

[22] Table 3 summarizes the height comparisons for ALL data. As expected, including the multilayered stratus and decks with holes increases the biases and standard deviations in cloud top height slightly for all cases except for Aqua at night. On average, the mean bias for ALL data is −0.587 km compared to −0.527 km for the SL data. The

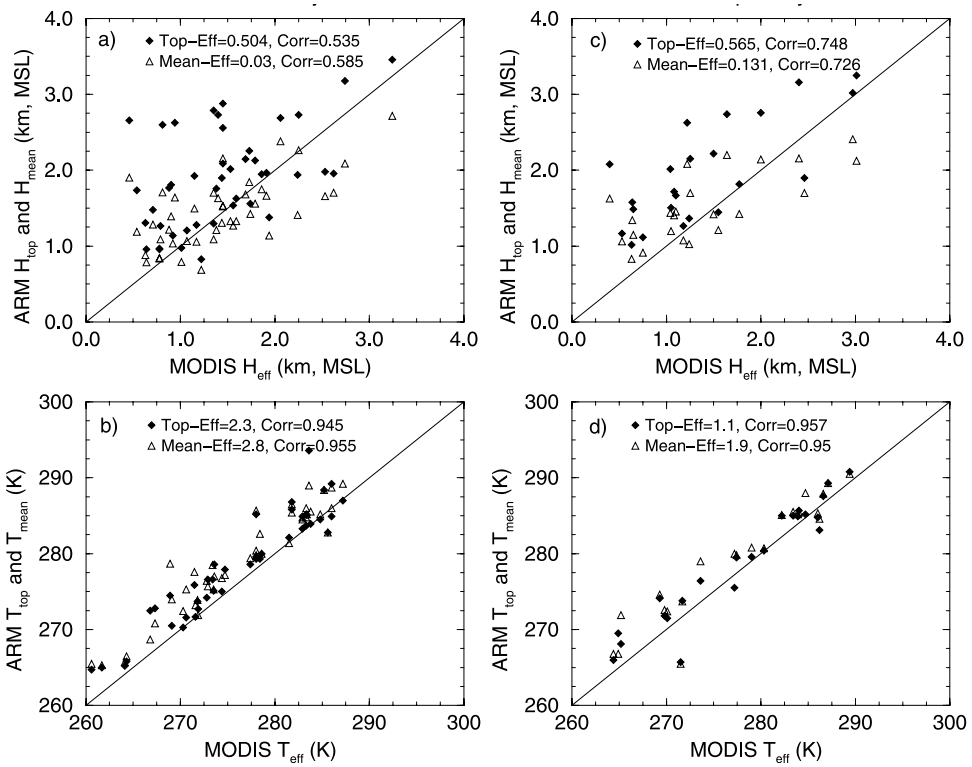

Figure 2. (a–d) Same as Figure 1 except for scatterplots.

standard deviation in the differences increases by 0.02 km from 0.556 km for the SL data. These height difference increases are accompanied by a smaller mean temperature difference and an increase in the temperature difference standard deviation.

3.2. Daytime Cloud Microphysical Property Comparisons

[23] The number of cases used in the SL daytime cloud microphysical property comparison is slightly less (e.g., 10 and 2 fewer samples for Terra and Aqua, respectively) than that for the cloud height and temperature comparisons because the clouds do not meet the surface retrieval criteria. The number samples for the daytime ALL data is also reduced. The surface-retrieved cloud microphysical properties are compared with the matched daytime Terra and Aqua SL samples in Figures 5 and 6. The means and standard deviations of the differences between Terra and Aqua results relative to the surface retrievals are summarized in Table 4 for both the SL (top) and ALL (bottom) data sets. In spite of the large differences in temporal and spatial resolution between surface and satellite, the time series of daytime SL VISST-retrieved r_e, τ, and LWP values from Terra have an excellent agreement with the surface retrievals with high correlations ($\sim$0.88) in τ and LWP and a modest correlation (0.44) in r_e. The correlations for ALL data are similar. The standard deviations in the satellite retrievals (not shown for sake of clarity) typically encompass the surface-derived values. For Aqua, the comparisons are very similar to their Terra counterparts except that the VISST yields greater

Table 2. Means and Standard Deviations (SD) of Differences and Linear Correlation Coefficients (Corr) of MODIS-Retrieved Effective Cloud Height and Temperature Relative to Surface-Observed Cloud Height and Temperature for SL Data (Samples Used in Figures 1–4)

		$H_{eff}-H_{base}$			$H_{eff}-H_{mean}$			$H_{eff}-H_{top}$		
	Number of Samples	Mean, km	SD, km	Corr	Mean, km	SD, km	Corr	Mean, km	SD, km	Corr
Terra, day	43	0.445	0.489	0.636	−0.030	0.484	0.585	−0.504	0.610	0.535
Aqua, day	23	0.333	0.636	0.50	−0.131	0.508	0.726	−0.565	0.498	0.748
Terra, night	22	0.150	0.501	0.696	−0.219	0.480	0.717	−0.587	0.549	0.662
Aqua, night	24	0.378	0.594	0.555	−0.050	0.439	0.753	−0.479	0.511	0.715
		$T_{eff}-T_{base}$			$T_{eff}-T_{mean}$			$T_{eff}-T_{top}$		
	Number of Samples	Mean, K	SD, K	Corr	Mean, K	SD, K	Corr	Mean, K	SD, K	Corr
Terra, day	43	−3.34	3.07	0.907	−2.80	2.13	0.955	−2.25	2.36	0.945
Aqua, day	23	−2.68	3.31	0.910	−1.89	2.45	0.95	−1.1	2.28	0.957
Terra, night	22	−2.45	3.07	0.93	−2.53	2.03	0.966	−2.45	1.91	0.966
Aqua, night	24	−3.91	5.33	0.70	−3.40	3.15	0.863	−2.90	2.75	0.90

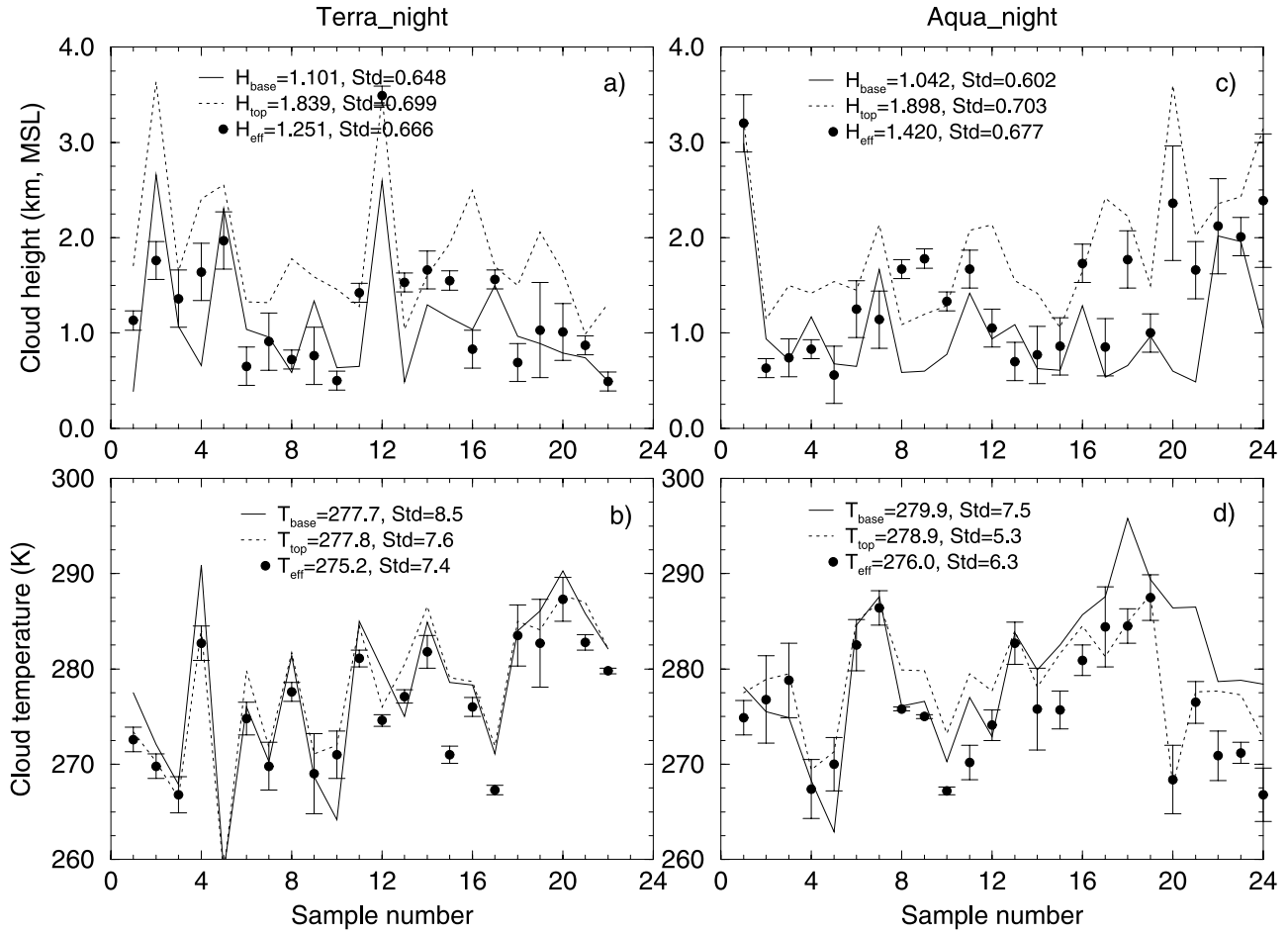

Figure 3. (a–d) Same as Figure 1 except for nighttime results.

values than those from the surface for LWP > 200 gm^{-2} (Figure 6f). On average, the means and standard deviations of the differences between the SL MODIS and surface values of r_e, τ, and LWP are 1.2 ± 23.5%, −3.6 ± 26.2%, and 0.3 ± 27% for Terra, and 2.5 ± 23.4%, 7.8 ± 24.3%, and 17.2 ± 32.2% for Aqua, respectively. The differences are similar for the ALL data set, except for the Aqua LWP, which is more biased and has a greater standard deviation compared to the SL data. All surface and MODIS retrievals, except for the MODIS-retrieved r_e, represent either total column (e.g., τ and LWP) or column mean (e.g., r_e), which can partially explain the high correlations in τ and LWP and modest correlations in r_e. The MODIS-retrieved r_e values (at 3.7-μm channel) represent the cloud top microphysical properties (at $\tau_{vis} \approx 3$ down into the cloud from the cloud top), while the ARM-retrieved r_e values are column means. Therefore the r_e differences in Figures 5a and 6a are likely to be caused by the difference between cloud top and layer mean r_e values.

4. Discussion

[24] While a full end-to-end discussion about the surface-satellite comparison is beyond the scope of this paper, the major elements of such an analysis are discussed in this section.

4.1. Cloud Height and Temperature Comparisons

[25] The differences in cloud heights and temperatures seen above are the result of many factors. In this section, we focus on the following three factors, which mainly affect the MODIS-derived cloud heights. The three factors are (1) emission arising from some depth within the cloud, (2) the choice of temperature profile, and (3) cloud top structure.

4.1.1. Dependence of H_{eff} on LWC Profile

[26] To illustrate the importance of the cloud microphysical properties to the MODIS measured T_{eff} and converted H_{eff}, consider Figure 7. The radiating level of the cloud (from satellite point of view) can be examined more quantitatively by considering the behavior of cloud emittance as a function of cloud thickness ΔZ and cloud liquid water content LWC. *Garrett et al.* [2002] used a Mie scattering code to calculate water cloud emittance ε at 11 μm based on the following equations:

$$\varepsilon_{11} = 1 - \exp(-\beta_{11}\tau_{abs}), \tag{3a}$$

$$\beta_{11} = 1.766 + 0.037 \exp\left(-\frac{r_e - 3.7}{4.96}\right), \tag{3b}$$

where the diffusion factor β_{11} is weakly dependent on r_e, and equals 1.7764 at r_e = 10 μm. The relationship between

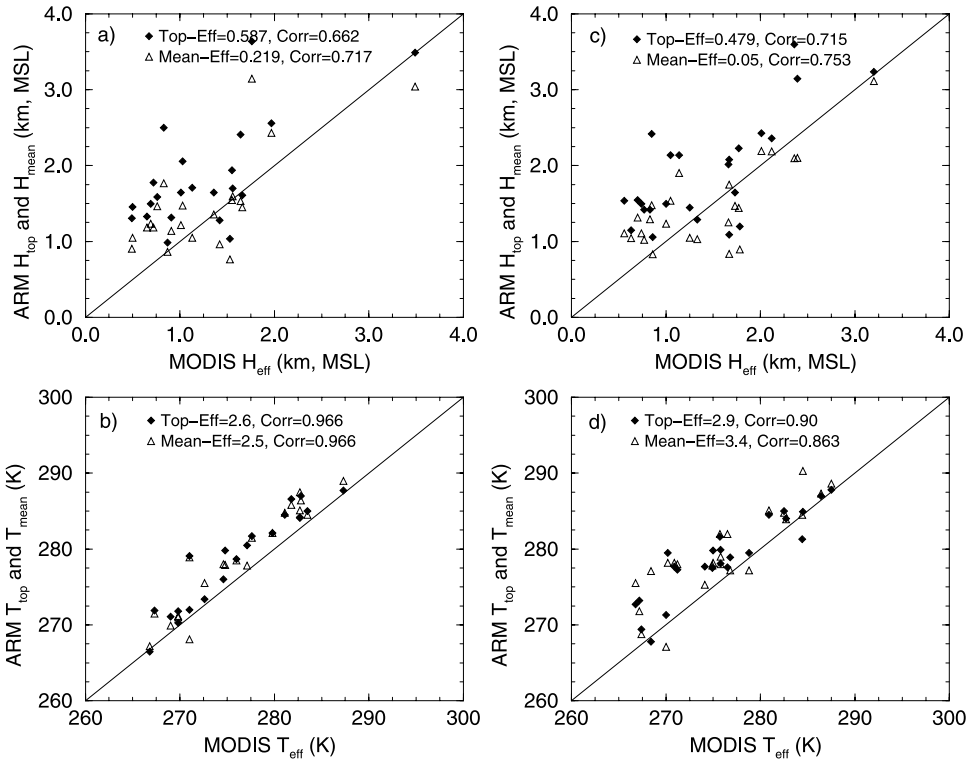

Figure 4. (a–d) Same as Figure 3 except for scatterplots.

τ, LWP and r_e was used to derive ε as a function of LWC and ΔZ (Figure 7) from equation (3) with fixed $r_e = 10$ μm and a scattering efficiency ratio $\xi_a (= \tau_{vis}/\tau_{abs} = 2.3)$ at $\lambda = 11$ μm [*Minnis et al.*, 1993a]. The emittances shown in Figure 7 are sensitive to r_e values when ε is significantly less than unity, and the estimates of the associated cloud thickness differ by ~50 m when r_e ranges from 5 to 15 μm. Emittance also depends on VZA [*Minnis et al.*, 1993a]. Assuming that satellite-observed stratus clouds are nearly blackbodies ($\varepsilon \sim 1$), Figure 7 shows that the stratus cloud radiative centers increase from 100 to 500 m from the cloud top when LWC reduces from 0.5 to 0.1 g m^{-3}.

[27] To further demonstrate the dependence of H_{eff} on LWC, Figure 8 shows LWC profiles for 8 cases selected from Figures 1–4. The LWC profiles were derived from the ARM radar-lidar-radiometer measurements as in the work by *Dong and Mace* [2003] and the means and standard deviations ($\pm 1\sigma$) are retrieved from the satellite retrievals. The H_{eff} values in Figures 8a and 8b are about 100 m below the cloud tops when their maximum LWCs are 0.45 g m^{-3}, those in Figures 8c–8e are approximately 300–500 m below their corresponding cloud tops when their LWCs range from 0.1 to 0.2 g m^{-3}, and the H_{eff} values in Figures 8f–8h are near the cloud bases when their LWCs are very small (~0.05 g m^{-3}). For these 8 cases, the mean difference between H_{top} and H_{eff} computed from equation (3) is 0.399 km with $\sigma = 0.293$ km. Assuming that these cases are representative, a significant portion of the mean difference and some of the variability in the differences is clearly due to the location of the radiating center of the cloud; it is

Table 3. Means and Standard Deviations (SD) of Differences and Linear Correlation Coefficients (Corr) of CERES-MODIS-Retrieved Effective Cloud Height and Temperature Relative to Surface-Observed Cloud Height and Temperature for ALL Data (Original Samples, Including Multilayer and Broken Clouds)

		$H_{eff}-H_{base}$			$H_{eff}-H_{mean}$			$H_{eff}-H_{top}$		
	Number of Samples	Mean, km	SD, km	Corr	Mean, km	SD, km	Corr	Mean, km	SD, km	Corr
Terra, day	64	0.369	0.509	0.436	−0.082	0.495	0.50	−0.534	0.655	0.394
Aqua, day	45	0.125	0.557	0.567	−0.274	0.512	0.651	−0.673	0.597	0.608
Terra, night	36	0.060	0.468	0.825	−0.309	0.487	0.803	−0.678	0.637	0.70
Aqua, night	33	0.320	0.564	0.694	−0.075	0.42	0.827	−0.471	0.481	0.80
		$T_{eff}-T_{base}$			$T_{eff}-T_{mean}$			$T_{eff}-T_{top}$		
	Number of Samples	Mean, K	SD, K	Corr	Mean, K	SD, K	Corr	Mean, K	SD, K	Corr
Terra, day	64	−2.95	3.15	0.924	−2.37	2.55	0.955	−1.77	2.81	0.943
Aqua, day	45	−2.26	2.95	0.916	−1.63	2.89	0.92	−1.02	3.52	0.877
Terra, night	36	−2.46	3.02	0.93	−2.31	2.44	0.952	−1.797	3.07	0.923
Aqua, night	33	−3.61	4.8	0.753	−3.1	2.91	0.896	−2.61	2.54	0.922

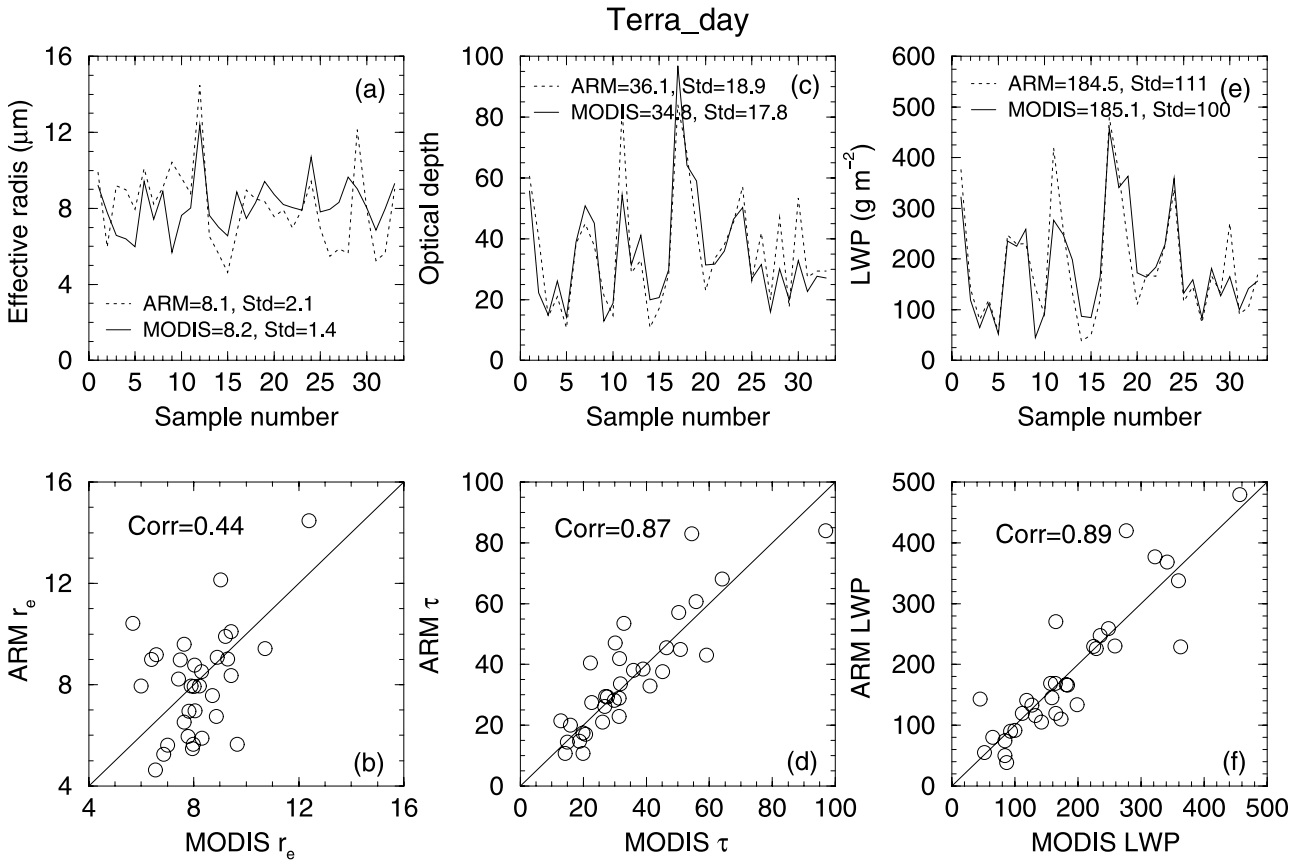

Figure 5. Time series of surface-derived (1-h average) and matched Terra and Aqua MODIS-derived cloud parameters (30 km × 30 km average), (a and b) cloud-droplet effective radius, (c and d) optical depth, and (e and f) LWP, for daytime single-layer and overcast stratus clouds over the ARM SGP site.

always located some distance below cloud top that varies according to the LWC profile. It is clear that an empirical correction should be applied to the water-cloud heights in the future.

4.1.2. Dependence of H_{eff} on Temperature Profile

[28] The remaining differences are due to conversion of T_{eff} to altitude, residual cirrus contamination, spatial variability, and correction of the water vapor attenuation of the 11-μm channel. In the stratus cloud cases, the latter is random and less than 0.10 km (Table 1) because the atmosphere above the single-layered stratus clouds is generally dry. Most cirrus-contaminated cases should have been eliminated in the secondary filtering of the data sets. Thus the largest concern is translating T_{eff} to a height. The temperature profiles in Figure 8 demonstrate how complicated the relationship between temperature and height can be. The minimum temperature, 283.5 K, in Figure 8a occurs twice, one near cloud base and 1 km above cloud top, while the actual top occurs within the inversion layer at temperature that is also found below cloud base. Sometimes part of the cloud is in the inversion and part is outside of it (Figures 8d–8h). No inversion is seen in Figure 8c, while double inversions occur in Figures 8b, 8d, 8e, and 8h. It is clear from these plots that assigning the proper altitude to an observed radiometric temperature using the traditional method, even if it occurs at cloud top in the profile, is fraught with uncertainty. The complicated structures of these boundary layer cloud systems often do not have a unique relationship between temperature and height.

4.1.2.1. Lapse Rate Versus Temperature Profile

[29] The method used for CERES is clearly a departure from the more traditional method, which begs the question: would the more traditional approach have yielded more accurate cloud heights than the lapse rate method? For a negative lapse rate, $T_{eff} < T_{top}$ indicates that H_{eff} should be higher than H_{top}. However, the lapse rate technique used for the CERES retrieval is inherently different from the use of the ARM sounding to convert H_{top} to T_{top}. If the traditional sounding conversion approach were optimal, then T_{eff} should be greater than or equal to T_{top}. Since $T_{eff} < T_{top}$, on average, then T_{top} occurs too high in the sounding as discussed in section 2.2.1.

[30] To quantitatively determine whether H_{eff} would have been closer to H_{top} if temperature profiles had been used, three experiments were conducted converting T_{eff} to H_{eff} using different temperature profiles over the ARM site. The first experiment degrades the merged ARM soundings to simulate the 25-hPa resolution of the GEOS profiles in the lower troposphere. To examine the impact of the resolution degradation, the second experiment employs the closest original high-resolution (25–40 m) ARM soundings that were taken within 3 h of the satellite overpass. The third experiment uses the 6-hourly GEOS 4.03 profiles interpolated to the overpass time. Table 5 summarizes the exper-

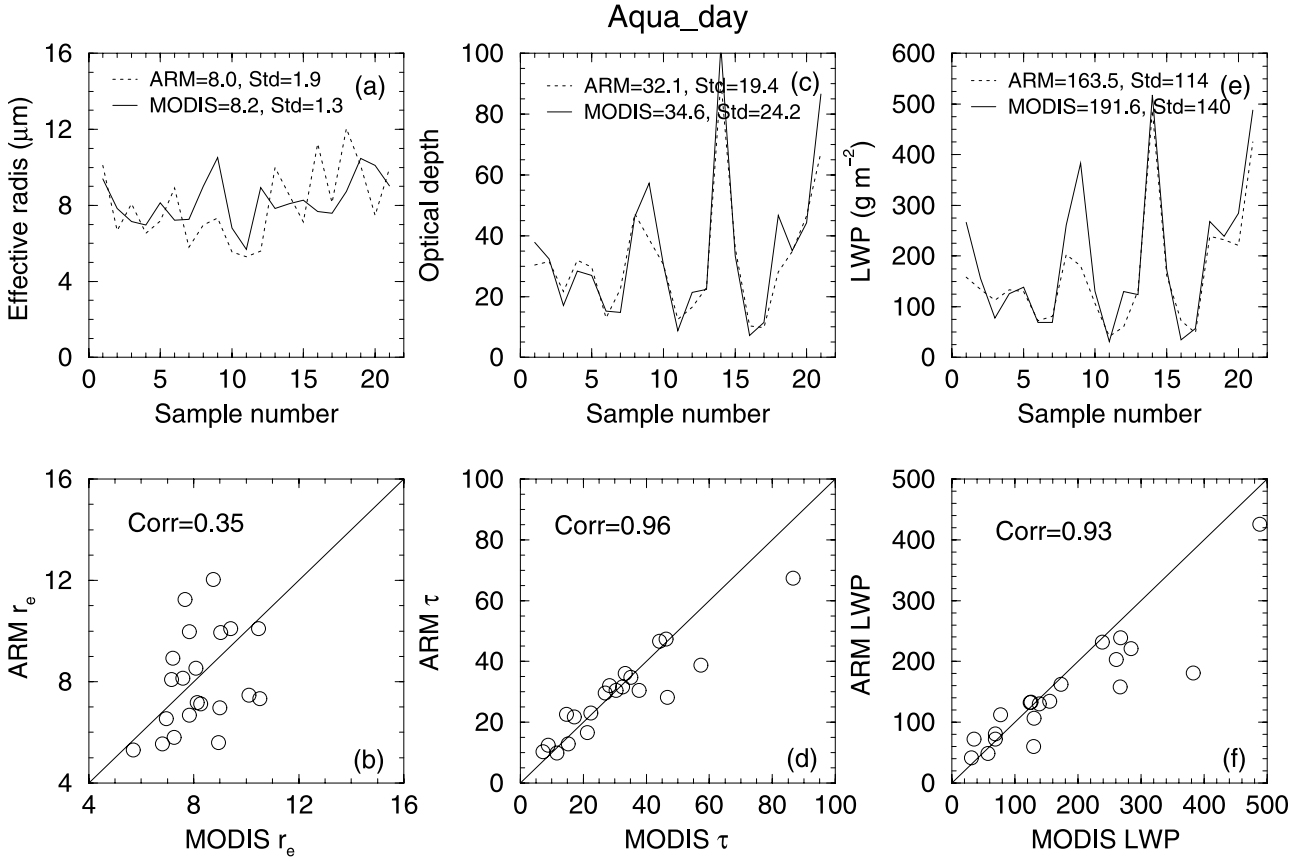

Figure 6. (a–f) Same as Figure 5 except for daytime Aqua results.

iment results for day and night using both SL and ALL data and compares them to those from the lapse rate method. In both experiments using the ARM soundings, H_{eff} overestimates H_{top} by ~0.63 km compared to the underestimate of ~0.55 km by the lapse rate approach. In addition to reversing the sign of the bias, both experiments significantly increase the SD of the differences compared to those for the lapse rate technique. Overall, the GEOS-like soundings increase the SDs by 76 and 72%, respectively, for the SL and ALL data sets. Surprisingly, the actual GEOS profiles yielded the smallest biases, ~0.38 km, overall. The accompanying difference SDs are comparable to those based on the ARM soundings. It is not clear why the GEOS 4.03 profiles yield results that are the same as, or possibly even better than, the original soundings. Since the GEOS 4.03 includes the ARM soundings in its assimilation, it likely produces profiles comparable to the original soundings and performs a more realistic interpolation between them than the linear interpolation method used for the merged soundings. Fidelity of the GEOS 4.03 temperatures to those in the actual profiles over areas lacking nearby radiosonde soundings is likely to be less than at locations, such as the ARM site, where the input soundings are taken. A concomitant degradation in the resulting values of H_{eff} in those areas would also be expected.

[31] The biases resulting from using the sounding methods clearly confirm that the observed cloud temperatures are, on average, not captured even in the original ARM soundings and explain why $T_{eff} < T_{top}$ determined from the MMCR heights. The lack of colder temperatures in the soundings at cloud top could be due to radiosonde lag effect noted earlier [*Mahesh et al.*, 1997] or to the cloud being

Table 4. Means and Standard Deviations (SD) of Differences and Linear Correlation Coefficients (Corr) of Daytime MODIS Retrievals Relative to Surface Results

		r_e(CERES)−r_e(sfc)			τ(CERES)−τ(sfc)			LWP(CERES)−LWP(sfc)		
SL	Number of Samples	Mean, μm	SD, μm	Corr	Mean	SD	Corr	Mean, gm^{-2}	SD, gm^{-2}	Corr
Terra	33	0.10, 1.2%	1.90, 23%	0.44	−1.3, −3.6%	9.46, 26%	0.87	0.6, 0.3%	49.9, 27%	0.89
Aqua	21	0.20, 2.5%	1.87, 23%	0.35	2.5, 7.8%	7.8, 24%	0.96	28.1, 17%	52.7, 32%	0.93
ALL										
Terra	54	−0.22, −2.8%	1.98, 25%	0.44	−1.72, −5.9%	7.92, 26%	0.91	−3.61, −2.4%	46.72, 31%	0.91
Aqua	44	0.34, 4.2%	1.99, 25%	0.39	2.55, 6.8%	6.58, 26%	0.96	32.68, 25%	63.77, 49%	0.91

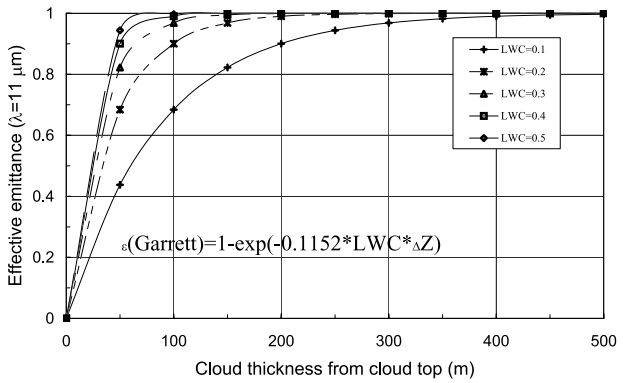

Figure 7. Sensitivities of water cloud emittance to cloud liquid water content LWC and cloud thickness from cloud top.

colder than its environment. An inversion above H_{top} would cause the former effect. Inversions occurred at H_{top} 55% and 46% of the time for nighttime Terra and Aqua, and 30% and 17.4% for daytime Terra and Aqua, respectively, in this study. Detailed study of the inversion impacts or the possible cloud-environment temperature differential effects should be examined in future studies.

[32] Considering all four data sets in Table 5, the magnitudes of the biases are not different at the 95% confidence level. Even if the 0.1–0.2 km reduction in the bias gained using the GEOS 4.03 temperature profile interpolation approach were significant, it would come at the cost of a dramatically increased instantaneous uncertainty. Furthermore, if a correction were made for the cloud radiating height, as discussed above, the bias would increase several hundred meters.

[33] Retrieving a low-cloud height with an accuracy better than ±1 km is a difficult task, at least in the midlatitudes and polar regions because of the complex structure of the lower troposphere, where positive lapse rates sometimes occur with in the cloud layer as seen in Figure 8. A reduction in the bias was the primary motivation for using the lapse rate technique over land for CERES Edition 2 processing. As noted earlier, during the initial testing, the lapse rate used over ocean was found to eliminate the bias over the SGP. Unfortunately, surface elevation was not taken into account when comparing the MMCR-derived and lapse rate cloud top heights. Accounting for the 0.32-km surface height in the testing would have produced results similar to those found here and likely would have led to an adjustment of the lapse rate prior to the Edition-2 processing. To minimize the bias over the SGP site, a lapse rate of -5.1 K km^{-1}, the averaged lapse rate below cloud top for 10 years of soundings over the ARM SGP site, would need to be used. Its applicability to other regions besides the SGP, however, needs further study. Nevertheless, the lapse rate approach used for the CERES processing significantly reduces the instantaneous error over the SGP and, with future reductions in the bias via emissivity corrections and a different lapse rate, would provide a more accurate approach than using profiles from numerical weather analyses.

4.1.2.2. Impact of Surface Temperature

[34] As evident in equation (2), the value of H_{eff} is sensitive to both lapse rate Γ and surface air temperature T_0. The sensitivity to lapse rate, $\Delta H_{eff}/H_{eff} \sim -\Delta\Gamma/\Gamma$, was discussed in section 2.2.3. As noted in the previous section, the optimal lapse rate for directly converting T_{eff} to H_{eff} is -5.1 K km^{-1}, assuming T_o is correct. An overestimate of T_o will result in an overestimate of H_{eff}, if lapse rate is correct, while the opposite is true for an underestimate of T_o. A total of 50 cases (out of 112 cases in Figures 1–4) fall out of the ARM-derived cloud boundaries. There are three methods to correct the 50 H_{eff} values in Figures 1–4 (i.e., the new H_{eff} falls within the ARM-derived cloud boundaries) by changing one or two parameters in equation (2). Out of the 50 cases, 24 (48%) can be corrected by using the ARM surface air temperature T(ARM), the MODIS-derived T_{eff}, and the fixed $\Gamma = -7.1$ K km^{-1}, instead of the GEOS surface air temperature T_0; 7 cases (14%) can be corrected by using ARM-derived lapse rate instead of the fixed $\Gamma = -7.1$ K km^{-1}; and 9 cases (18%) can be corrected by using both T(ARM) and new lapse rate. There are only 10 cases (out of the 50 cases, 20%) that cannot be corrected by the above three methods. Therefore the uncertainty in T_o is also a contributor leading to the random errors in the heights derived from the satellite data.

4.1.3. Spatial-Temporal Variation

[35] There are a few cases in Figures 1–4 with large standard deviations that should not be due to broken and/or multilayer clouds because the cases used in this study are solid single-layer and overcast clouds. A careful examination of the ARM radar and satellite images reveals that the large standard deviations are mainly caused by large variations in cloud top height. Figure 9 shows the 5-min cloud base and cloud-top heights and temperatures derived from ARM observations and MODIS means and standard deviations ($\pm 1\sigma$) of H_{eff} (the cases 1 and 2 in Figure 1b). The cloud top heights vary from 2 km to 4 km, and cloud top temperatures range from 271 to 285 K. Similar variations are seen in the satellite results. Height differences introduced by such cloud top height variability are apparently no worse than those resulting from having some holes in the cloud field, optical depths less than 10, or multilayered stratus layers, given small increases in the biases and SDs for the ALL data in Table 3 relative to the SL cases in Table 2.

4.2. Microphysical Properties

[36] Except for the Aqua-derived LWP values, the good agreement between the surface and CERES-MODIS cloud microphysical properties and high level of correlation in cloud τ and LWP for both SL and ALL data indicate that VISST can provide accurate and reliable retrievals of these parameters for most of the overcast stratus clouds. The modest correlations in r_e and lack of a significant bias, however, are puzzling.

4.2.1. Daytime Cloud Droplet Sizes

[37] In addition to the uncertainties listed in Table 1, spatial-temporal variations as well as the vertical variability of droplet size will introduce differences between the surface- and satellite-derived values of r_e. The differences in r_e between the actual clouds sampled by the ARM sensors over a fixed time period and those sampled instan-

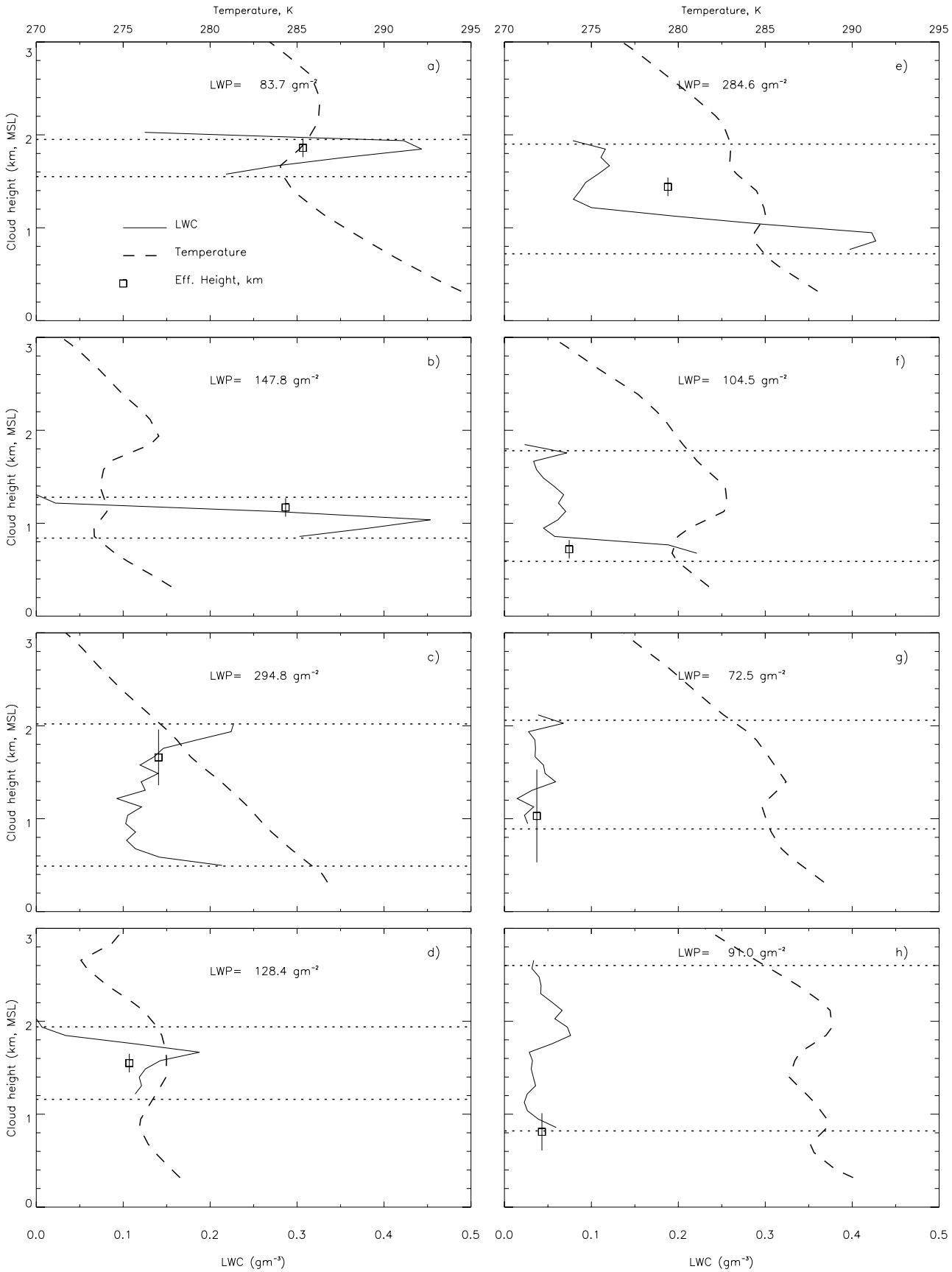
Temperature, K
270
275
280
285
290
295
a)
LWP= 83.7 gm⁻²
LWC
Temperature
Eff. Height, km
e)
LWP= 284.6 gm⁻²
b)
LWP= 147.8 gm⁻²
f)
LWP= 104.5 gm⁻²
c)
LWP= 294.8 gm⁻²
g)
LWP= 72.5 gm⁻²
d)
LWP= 128.4 gm⁻²
h)
LWP= 91.0 gm⁻²
Cloud height (km, MSL)
0
1
2
3
0.0
0.1
0.2
0.3
0.4
0.5
LWC (gm⁻³)

Figure 8

Table 5. Comparison of Cloud Height Differences Using Different Temperature-to-Height Conversion Techniques Using Aqua and Terra Data as in Tables 2 and 3

	Samples		H_{top}, km		$H_{eff}-H_{top}$, km		$SD(H_{eff}-H_{top})$, km	
Method	SL	All	SL	All	SL	All	SL	All
Lapse rate	66	109	1.924	1.912	−0.504	−0.592	0.598	0.638
Merged sounding	66	109	1.924	1.912	0.550	0.494	1.010	1.087
ARM sounding	34	59	1.997	2.029	0.669	0.493	0.91	1.101
GEOS 4.03	66	109	1.92	1.912	0.396	0.378	0.971	1.086
Lapse rate	46	69	1.870	2.007	−0.531	−0.579	0.538	0.582
Merged sounding	46	69	1.870	2.007	0.612	0.573	0.994	0.953
ARM sounding	23	35	1.806	2.049	0.718	0.629	0.834	0.823
GEOS 4.03	46	69	1.87	2.01	0.387	0.368	1.030	1.014

taneously by the satellite over a large area introduces a random horizontal error in the comparisons, while the vertical variations tend to produce a bias. Typically, the satellite-retrieved value of r_e (e.g., using 3.7-μm channel) is representative of cloud particle size near the cloud top for optically thick clouds [e.g., *Nakajima and King*, 1990], while the surface-retrieved r_e, weighted by water mass in the cloud, represents the layer mean particle size. In most instances, droplet size increases with height in the cloud and r_e at the top should typically overestimate the value for the entire cloud. However, r_e may decrease with height if there is light drizzle near the cloud base and/or strong entrainment near the cloud top. Although the mean differences in both Terra and Aqua comparisons are very small, the differences for some individual cases are large. Therefore it is necessary to investigate the r_e vertical distributions for those cases.

[38] Figure 10 presents r_e vertical profiles derived from the MMCR and MWR data using the technique of *Dong and Mace* [2003]. They represent four conditions: (1) increasing with height; (2) decreasing with height; (3) increasing first, then decreasing; and (4) random variation. Although these four types of vertical distributions cannot represent all conditions and even cannot explain some of those cases with large differences in Figures 5 and 6, they represent a wide range of the vertical distributions. Together, with the other uncertainties, they can account for the small differences in mean r_e despite the modest correlation. Sometimes, the satellite retrieval will be larger than the surface-based value because the cloud top has larger droplets and, in other cases, the reverse will occur because the cloud top has smaller droplets than the rest of the cloud. Comparing the MODIS-retrieved r_e values, shown in Figure 10, with those 100–400 m below cloud top in the r_e profiles reveals very good agreement even though the results may not agree in Figures 5 and 6. It is concluded that the overall excellent agreement, the lack of bias, between ARM and MODIS r_e retrievals is mainly due to the combination of different types of r_e vertical distributions found in these samples.

4.2.2. Daytime Cloud Optical Depth and Liquid Water Path

[39] Relative to the surface measurements, the mean optical depths retrieved from Aqua are greater than those from Terra by 3.8 (11.4%) for the SL and 4.3 (12.7%) for ALL observations (Table 4). These relative differences are significant, at least, at the 1-σ level. While these differences may be due to differences in the clouds, at least, part of the discrepancy is due to the calibration differences. *Minnis et al.* [2008] found that the VIS channel gain on Aqua is 1% greater than that on Terra prior to October 2003 and 2.1% greater thereafter. This calibration difference will cause only negligible differences for $\tau < 10$, but would be increasingly important at larger optical depths. For example, for $\tau = 32$ and $r_e = 8$ μm at SZA = 41°, the Aqua reflectance would yield optical depths of 34.3 and 37.1 compared to 32 for Terra before and after October 2003, respectively. For the SL cases, this difference translates 11.6%, which is statistically the same as the 11.4% relative difference in Table 4. Accounting for the relative differences in calibration before and after October 2003 for each sample in the ALL data would reduce the mean Aqua optical depth by 1.7, resulting in an average difference of 0.8 compared to the surface results. The adjusted mean differences between the Aqua and Terra satellite-surface biases then would not be statistically different. Thus it is concluded that the calibration differences between the two satellite VIS channels could explain the mean relative differences seen in the satellite-surface comparisons. It is not clear which of the two channels has a more accurate absolute calibration.

[40] Because LWP is a product of τ and r_e, the LWP errors arise from errors in the other two quantities. Thus, when either r_e or τ is underestimated or overestimated, LWP will follow. In some instances, errors in either variable can cancel each other leading to a good estimate of LWP or they can compound each other leading to extreme errors. This could explain why the bias and SD in the Aqua LWP are so much greater than those found for Terra. Coincident over-

Figure 8. Cloud boundaries (dotted lines), LWC (solid), LWP, and temperature (dashed) derived from ARM radar-lidar-radiometer measurements and merged soundings; and the CERES-MODIS-derived means and standard deviations (vertical bars) of effective heights. (a and b) With high LWCs of 0.4–0.5 gm^{-3}, (c–e) with average LWCs of 0.1 to 0.2 gm^{-3}, and (f–h) with low LWCs of 0–0.1 gm^{-3}. The surface data were averaged over a 1-h interval centered at the time of the satellite overpass, and the satellite data were averaged within a 30 km × 30 km area centered on the ARM SGP site.

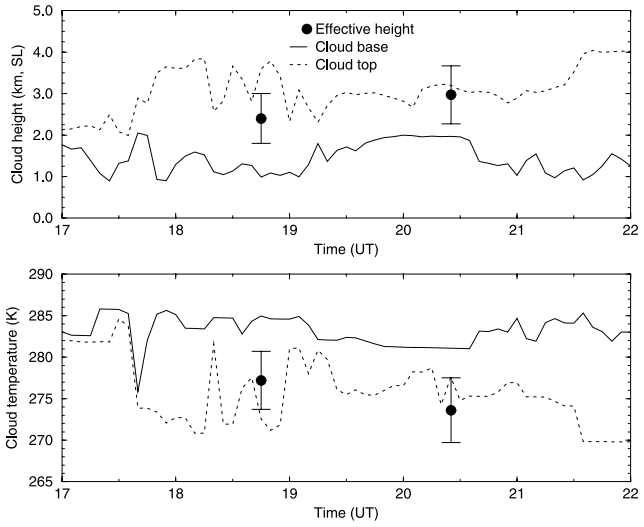

Figure 9. The 5-min cloud base and cloud-top heights and temperatures measured at the ARM SGP site for the cases 1 and 2 (19 September 2002) in Figure 1b. The means and standard deviations ($\pm 1\sigma$) are derived from MODIS data.

estimates of τ and r_e for large values of τ (Figure 6) would cause extreme overestimates in LWP. These individual overestimates could be compensated by underestimates in τ and r_e in separate samples that result in only minor underestimates in LWP that do not balance the extreme anomalies. The discrepancies in the Aqua and Terra relative LWP differences would be reduced somewhat if their calibrations were normalized.

[41] When comparing the satellite and surface-based quantities, there is always some mismatch in terms of the actual portions of the clouds that are sampled. The time average of the clouds sampled by the small-beam radar and variable field of view (depends on cloud base height) is assumed to provide a value that is represented by the spatial average of the relatively large imager pixels. A more precise match of the data could have been attempted by using "wind strips" of satellite pixels. Those strips of pixels correspond to the clouds advecting over the site during the averaging period of the surface instruments. As found by *Dong et al.* [2002], however, the more precise "strips" approach yields nearly the same statistics as the simple "box" average used here, presumably because there is no assurance that the relatively large pixels are represented by

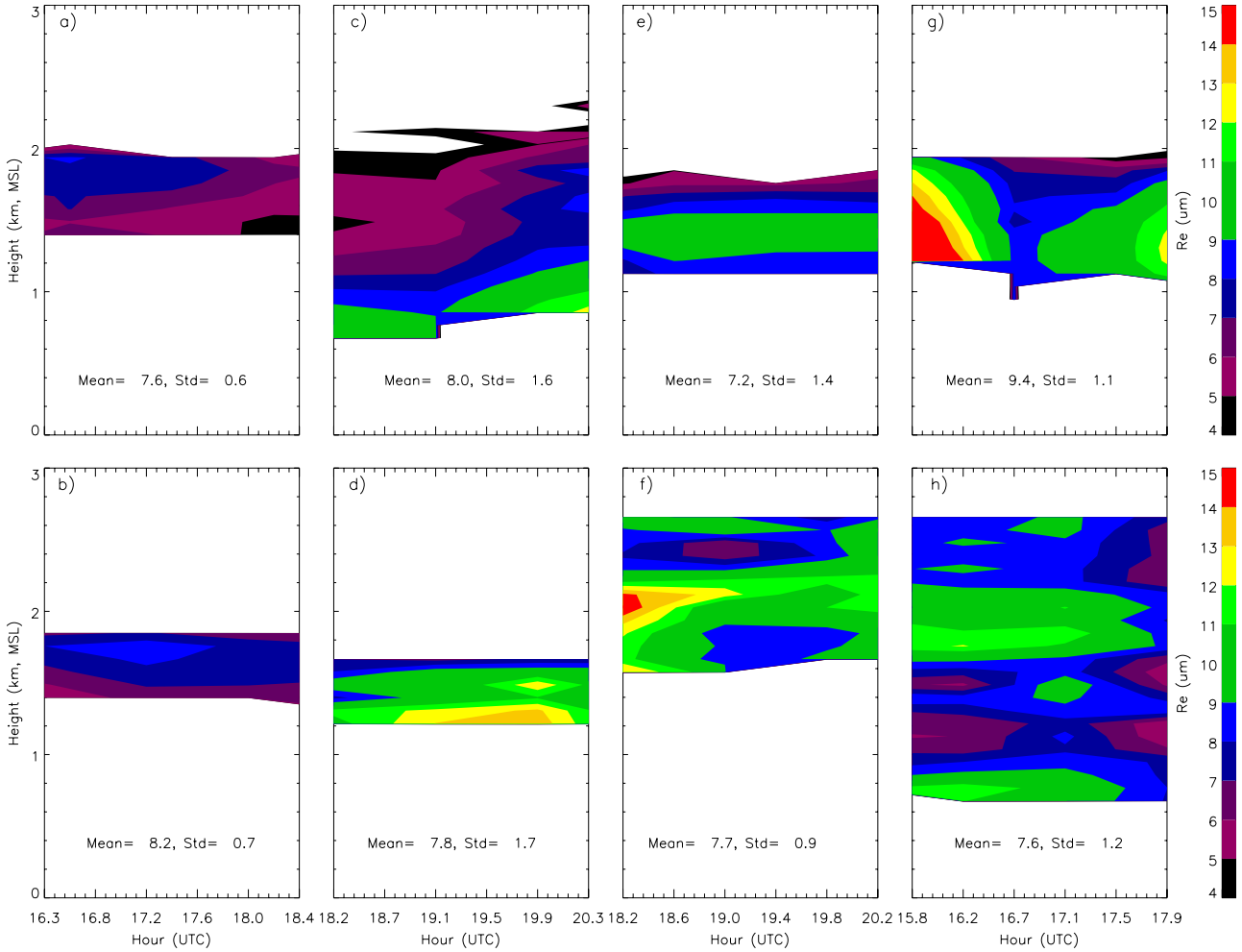

Figure 10. The 5-min ARM radar derived r_e profiles [*Dong and Mace*, 2003] plotted ±1 h centered at satellite overpass the ARM SGP site. The means and standard deviations are derived from MODIS 3.7-μm channel.

the beam averages on a one-to-one basis. Thus the VISST values used here should be suitable for making the comparisons.

[42] Nevertheless, some spatial-temporal sampling errors will contribute to the random errors along with the uncertainties listed in Table 1. *Horváth and Davies* [2007] compared results from near-nadir MODIS standard atmospheric products [*Platnick et al.*, 2003], MOD06, to LWP derived from a satellite-borne microwave imager over ocean and found that the differences were within 5–10% on average, with an instantaneous uncertainty of 35% for overcast boundary layer clouds. Taking the Terra and Aqua results together, the mean SL LWP differences found here are less than or equal to those from that study, but the ALL LWP SD differences are larger by 5%. The ALL data are probably more like cases used by *Horváth and Davies* [2007]. A smaller SD would be expected for the satellite-to-satellite comparison because the data were spatially matched and differ in time by no more than 15 min. The significant spatial differences and larger time differences in the surface-satellite comparisons drive up the SD in the comparison of those quantities.

[43] An additional factor that influences the satellite retrievals is cloud top structure, like that seen in Figure 9. It will cause three-dimensional effects that result in reflectance patterns that deviate from the plane-parallel model used in the satellite retrievals. This impact is often evident in VZA dependencies. *Horváth and Davies* [2007] found a slight increase in LWP with VZA, ~20% at VZA between 60 and 70°. The CERES-ARM LWP difference increase with VZA is nearly identical, changing from 1% at VZA = 5° to 21% for VZA = 65°. Although there are too few samples to conclude that the trend is statistically significant, this effect will at a minimum contribute to the random error.

5. Conclusions

[44] Most of the daytime and nighttime MODIS-derived H_{eff} values are within the radar-lidar derived cloud boundaries. The CERES-MODIS effective cloud heights correspond most closely to the physical centers of the cloud being, on average, 0.108 ± 0.48 km below it. The value of H_{eff} underestimates the radar-derived cloud top height by 0.534 ± 0.542 km. No significant day-night difference was found in the analyses. Adding more cases with thinner, broken, or multilayer clouds, causes minor changes in the comparisons. While small, the degree of contamination in the rejected cases posed the potential of adding noise and biases that would compromise the comparisons in unpredictable ways. Consequently, these observations were removed. A sensitivity study has shown that a significant portion of the bias is due to the fact that H_{eff} does not correspond to cloud top, but rather to the radiating center of the cloud which can be various locations in the clouds due to LWC vertical distribution. The remaining bias is due to using a lapse rate that is not steep enough. Random variations in errors are due to a combination of spatial and temporal sampling differences, uncertainties in the GEOS surface air temperature and the assumed lapse rate. Despite the uncertainties, it concluded that the use of the lapse rate approach can provide a more accurate estimate of boundary layer cloud top height than the use of a temperature profile based on radiosonde data or numerical weather analyses.

[45] The good agreement between the surface and MODIS retrieved cloud microphysical properties and high level of correlation in cloud τ and LWP indicate that the temporally averaged surface observations are equivalent to the spatially averaged satellite results, that is, the uncertainty of spatial-temporal sampling noise is minimized in this study. The good agreement also reveals that VISST can provide accurate and reliable retrievals of these parameters for single-layer and overcast stratus clouds. The r_e comparison with modest correlation, however, involves both temporal-spatial match and vertical distribution of r_e. The overall excellent agreement in their averages between ARM and MODIS retrievals is mainly due to the combination of different types of r_e vertical distributions in this study.

[46] The results presented here represent only one class of clouds in a single area over a limited range of solar zenith angles. Without additional comparisons over other regions, it is not clear whether the current findings are representative of stratus clouds over land surfaces. More validation is needed for stratus clouds at different locations, such as polar, desert, and tropical regions, and also for different cloud types, including multilayered and broken clouds. Efforts are ongoing to address some of these other validation concerns, but the lack of fully instrumented surface sites in all climate regimes hampers this effort. Eventually, enough independent samples will be collected at the available sites to perform statistically significant surface-satellite comparisons for several different climate regimes and cloud types. Angular and diurnal dependencies in the satellite retrievals can also be evaluated with additional samples and with comparisons to other satellites, both polar-orbiting and geostationary. These limited site comparisons can be complemented on a global scale with new active sensors on satellites. With the 2006 launch of CloudSat and the Cloud-Aerosol Lidar and Infrared Pathfinder Satellite Observation satellite, it will be possible to perform similar comparisons globally using retrievals from Aqua MODIS thus giving the means to assess all cloud types over all regions at two local times and at one viewing zenith angle. Together with the surface measurements, these new data sources will provide the means to fully assess the errors in passive satellite cloud retrievals and the basis to make significant improvements in future editions of those retrieval algorithms.

[47] **Acknowledgments.** This research was supported by the NASA CERES project under grant NNL04AA11G at the University of North Dakota and by the ARM Program under interagency agreement DE-AI02-97ER62341. Special thanks to Sally Benson and Gerald G. Mace at University of Utah for providing preprocessed ARM cloud data.

References

Ackerman, T. P., and G. M. Stokes (2003), The Atmospheric Radiation Measurement Program, *Phys. Today*, *56*, 38–44.

Arduini, R. F., P. Minnis, and D. F. Young (2002), Investigation of a visible reflectance parameterization for determining cloud properties in multilayered clouds, paper presented at 11th Conference on Cloud Physics, Am. Meteorol. Soc., Ogden, Utah, 3–7 Jun.

Bloom, S., et al. (2005), Documentation and validation of the Goddard Earth Observing System (GEOS) Data Assimilation System–Version 4, *Tech. Rep. Ser. Global Model. Data Assim. 104606*, 26 pp., NASA Goddard Space Flight Cent., Greenbelt, Md.

Cess, R. D., et al. (1990), Intercomparison and interpretation of climate feedback processes in 19 atmospheric general circulation models, *J. Geophys. Res.*, *95*, 16,601–16,615.

Cess, R. D., et al. (1996a), Cloud feedback in atmospheric general circulation models: An update, *J. Geophys. Res.*, *101*, 12,791–12,794.

Cess, R. D., M. H. Zhang, Y. Zhou, X. Jing, and V. Dvortsov (1996b), Absorption of solar radiation by clouds: Interpretations of satellite, surface, and aircraft measurements, *J. Geophys. Res.*, *101*, 23,299–23,309.

Chiriaco, M., et al. (2007), Comparison of CALIPSO-like, LaRC, and MODIS retrievals of ice cloud properties over SIRTA in France and Florida during CRYSTAL-FACE, *J. Appl. Meteorol. Climatol.*, *46*, 249–272.

Clothiaux, E. E., T. P. Ackerman, G. G. Mace, K. P. Moran, R. T. Marchand, M. A. Miller, and B. E. Martner (2000), Objective determination of cloud heights and radar reflectivities using a combination of active remote sensors at the ARM CART sites, *J. Appl. Meteorol.*, *39*, 645–665.

Curry, J. A., et al. (2000), FIRE Arctic Clouds Experiment, *Bull. Am. Meteorol. Soc.*, *81*, 5–29.

Dong, X., and G. G. Mace (2003), Profiles of low-level stratus cloud microphysics deduced from ground-based measurements, *J. Atmos. Oceanic Technol.*, *20*, 42–53.

Dong, X., T. P. Ackerman, E. E. Clothiaux, P. Pilewskie, and Y. Han (1997), Microphysical and radiative properties of stratiform clouds deduced from ground-based measurements, *J. Geophys. Res.*, *102*, 23,829–23,843.

Dong, X., T. P. Ackerman, and E. E. Clothiaux (1998), Parameterizations of microphysical and shortwave radiative properties of boundary layer stratus from ground-based measurements, *J. Geophys. Res.*, *103*, 31,681–31,693.

Dong, X., P. Minnis, T. P. Ackerman, E. E. Clothiaux, G. G. Mace, C. N. Long, and J. C. Liljegren (2000), A 25-month database of stratus cloud properties generated from ground-based measurements at the ARM SGP site, *J. Geophys. Res.*, *105*, 4529–4538.

Dong, X., G. G. Mace, P. Minnis, and D. F. Young (2001), Arctic stratus cloud properties and their effect on the surface radiation budget: Selected cases from FIRE ACE, *J. Geophys. Res.*, *106*, 15,297–15,312.

Dong, X., P. Minnis, G. G. Mace, W. L. Smith Jr., M. Poellot, R. Marchand, and A. Rapp (2002), Comparison of stratus cloud properties deduced from surface, GOES, and aircraft data during the March 2000 ARM Cloud IOP, *J. Atmos. Sci.*, *59*, 3265–3284.

Garreaud, R. D., J. Rutllant, J. Quintana, J. Carrasco, and P. Minnis (2001), CIMAR-5: A snapshot of the lower troposphere over the subtropical southeast Pacific, *Bull. Am. Meteorol. Soc.*, *92*, 2193–2208.

Garrett, T. J., L. F. Radke, and P. V. Hobbs (2002), Aerosol effects on cloud emissivity and surface longwave heating in the Arctic, *J. Atmos. Sci.*, *59*, 769–778.

Greenwald, T. J., S. A. Christopher, J. Chou, and J. C. Liljegren (1999), Intercomparison of cloud liquid water path derived from the GOES-9 imager and ground-based microwave radiometers for continental stratus, *J. Geophys. Res.*, *104*, 9251–9260.

Han, Q., W. B. Rossow, and A. A. Lacis (1994), Near-global survey of effective droplet radii in liquid water clouds using ISCCP data, *J. Clim.*, *7*, 465–497.

Horváth, Á., and R. Davies (2007), Comparison of microwave and optical cloud water path estimates from TMI, MODIS, and MISR, *J. Geophys. Res.*, *112*, D01202, doi:10.1029/2006JD007101.

Houghton, J. T., et al. (2001), *Climate Change 2001: The Scientific Basis*, Cambridge Univ. Press, New York.

Kratz, D. P. (1995), The correlated *k*-distribution technique as applied to the AVHRR channels, *J. Quant. Spectrosc. Radiat. Transfer*, *53*, 501–517.

Liljegren, J. C., E. E. Clothiaux, G. G. Mace, S. Kato, and X. Dong (2001), A new retrieval for cloud liquid water path using a ground-based microwave radiometer and measurements of cloud temperature, *J. Geophys. Res.*, *106*, 14,485–14,500.

Mace, G. G., T. P. Ackerman, P. Minnis, and D. F. Young (1998), Cirrus layer microphysical properties derived from surface-based millimeter radar and infrared interferometer data, *J. Geophys. Res.*, *103*, 23,207–23,216.

Mace, G. G., Y. Zhang, S. Platnick, M. D. King, P. Minnis, and P. Yang (2005), Evaluation of cirrus cloud properties from MODIS radiances using cloud properties derived from ground-based data collected at the ARM SGP site, *J. Appl. Meteorol.*, *44*, 221–240.

Mahesh, A., V. P. Walden, and S. G. Warren (1997), Radiosonde temperature measurements in strong inversions: Correction for thermal lag based on an experiment at the South Pole, *J. Atmos. Oceanic Technol.*, *14*, 45–53.

Minnis, P., and E. F. Harrison (1984), Diurnal variability of regional cloud and clear-sky radiative parameters derived from GOES data, part II: November 1978 cloud distributions, *J. Clim. Appl. Meteorol.*, *23*, 1012–1031.

Minnis, P., P. W. Heck, D. F. Young, C. W. Fairall, and J. B. Snider (1992), Stratocumulus cloud properties derived from simultaneous satellite and island-based instrumentation during FIRE, *J. Appl. Meteorol.*, *31*, 317–339.

Minnis, P., Y. Takano, and K.-N. Liou (1993a), Inference of cirrus cloud properties using satellite-observed visible and infrared radiances, part I: Parameterization of radiance fields, *J. Atmos. Sci.*, *50*, 1279–1304.

Minnis, P., P. W. Heck, and D. F. Young (1993b), Inference of cirrus cloud properties using satellite-observed visible and infrared radiances, part II: Verification of theoretical cirrus radiative properties, *J. Atmos. Sci.*, *50*, 1305–1322.

Minnis, P., et al. (1995), Cloud Optical Property Retrieval (Subsystem 4.3). Clouds and the Earth's Radiant Energy System (CERES) Algorithm Theoretical Basis Document, volume III: Cloud Analyses and Radiance Inversions (Subsystem 4), *NASA Tech. Rep. RP 1376*, 135–176.

Minnis, P., D. P. Garber, D. F. Young, R. F. Arduini, and Y. Takano (1998), Parameterization of reflectance and effective emittance for satellite remote sensing of cloud properties, *J. Atmos. Sci.*, *55*, 3313–3339.

Minnis, P., et al. (2002), A global cloud database from VIRS and MODIS for CERES, *Proc. SPIE Int. Soc. Opt. Eng.*, *4891*, 115–126.

Minnis, P., W. L. Smith Jr., L. Nguyen, J. J. Murray, P. W. Heck, and M. M. Khaiyer (2003), Near-real-time satellite cloud products for icing detection and aviation weather over the USA, paper presented at In-Flight Icing/De-icing International Conference, Fed. Aviation Admin., Chicago, Ill., 16–20 Jun.

Minnis, P., et al. (2006), Overview of CERES cloud properties from VIRS and MODIS, paper presented at 12th Conference on Atmospheric Radiation, Am. Meteorol. Soc., Madison, Wis., 10–14 July.

Minnis, P., D. R. Doelling, L. Nguyen, W. F. Miller, and V. Chakrapani (2008), Assessment of the visible channel calibrations of TRMM VIRS and MODIS on Aqua and Terra, *J. Atmos. Oceanic Technol.*, in press.

Moran, K. P., B. E. Martner, M. J. Post, R. A. Kropfli, D. C. Welsh, and K. B. Widener (1998), An unattended cloud-profiling radar for use in climate research, *Bull. Am. Meteorol. Soc.*, *79*, 443–455.

Nakajima, T., and M. D. King (1990), Determination of the optical thickness and effective particle radius of clouds from reflected solar radiation measurements. Part I: Theory, *J. Atmos. Sci.*, *47*, 1878–1893.

Platnick, S., and F. P. J. Valero (1995), A validation of a satellite cloud retrieval during ASTEX, *J. Atmos. Sci.*, *52*, 2985–3001.

Platnick, S., M. D. King, S. A. Ackerman, W. P. Menzel, B. A. Baum, J. C. Riedi, and R. A. Frey (2003), The MODIS cloud products: Algorithms and examples from Terra, *IEEE Trans. Geosci. Remote Sens.*, *41*, 459–473.

Rossow, W. B., and R. A. Schiffer (1999), Advances in understanding clouds from ISCCP, *Bull. Am. Meteorol. Soc.*, *80*, 2261–2287.

Tobin, D. C., H. E. Revercomb, C. C. Moeller, and T. S. Pagano (2006), Use of Atmospheric Infrared Sounder high–spectral resolution spectra to assess the calibration of Moderate resolution Imaging Spectroradiometer on EOS Aqua, *J. Geophys. Res.*, *111*, D09S05, doi:10.1029/2005JD006095.

Trepte, Q., Y. Chen, S. Sun-Mack, P. Minnis, D. F. Young, B. A. Baum, and P. W. Heck (1999), Scene identification for the CERES cloud analysis subsystem, paper presented at 10th Conference on Atmospheric Radiation, Am. Meteorol. Soc., Madison, Wis., 28 June to 2 July.

Trepte, Q., P. Minnis, and R. F. Arduini (2002), Daytime and nighttime polar cloud and snow identification using MODIS data, *Proc. SPIE Int. Soc. Opt. Eng.*, *4891*, 449–459.

Wielicki, B. A., R. D. Cess, M. D. King, D. A. Randall, and E. F. Harrison (1995), Mission to planet Earth: Role of clouds and radiation in climate, *Bull. Am. Meteorol. Soc.*, *76*, 2125–2153.

Wielicki, B. A., B. R. Barkstorm, E. F. Harrison, R. B. Lee III, G. L. Smith, and J. E. Cooper (1996), Clouds and the Earth's Radiant Energy System (CERES): An Earth Observing System Experiment, *Bull. Am. Meteorol. Soc.*, *77*, 853–868.

Wielicki, B. A., et al. (1998), Clouds and the Earth's Radiant Energy System (CERES): Algorithm overview, *IEEE Trans. Geosci. Remote Sens.*, *36*, 1127–1141.

Wielicki, B. A., et al. (2000), CERES validation plan overview, release 4, 10/20/00, 58 pp., NASA Langley Res. Cent., Hampton, Va. (Available at http://asd-www.larc.nasa.gov/ceres/validation/ceresval_r4.0_over.pdf)

Y. Chen and S. Sun-Mack, Science Applications International Corporation, Inc., Hampton, VA 23666, USA.

X. Dong and B. Xi, Department of Atmospheric Sciences, University of North Dakota, 4149 University Drive, Stop 9006, Grand Forks, ND 58202-9006, USA. (dong@aero.und.edu)

P. Minnis, NASA Langley Research Center, Hampton, VA 23681, USA.